Global Biogeochemical Cycles®

RESEARCH ARTICLE
10.1029/2021GB007145

Key Points:

- Three algorithms are used to reconstruct air-sea gas fluxes of biological oxygen ($F_{[O_2]_{bio\text{-}as}}$) from dissolved oxygen
- Simultaneous measurements of O_2/Ar and O_2 concentration collected on 14 cruises are used to train and test the models
- The empirical equation based on ship-based measurements and historical physical records provides the most robust predictions

Supporting Information:

Supporting Information may be found in the online version of this article.

Correspondence to:

N. Cassar,
Nicolas.Cassar@duke.edu

Citation:

Huang, Y., Eveleth, R., Nicholson, D., & Cassar, N. (2022). Can we estimate air-sea flux of biological O_2 from total dissolved oxygen? *Global Biogeochemical Cycles*, *36*, e2021GB007145. https://doi.org/10.1029/2021GB007145

Received 5 AUG 2021
Accepted 10 AUG 2022

Can We Estimate Air-Sea Flux of Biological O_2 From Total Dissolved Oxygen?

Yibin Huang[1,2,3], Rachel Eveleth[1,4], David Nicholson[5], and Nicolas Cassar[1,6]

[1]Division of Earth and Climate Sciences, Nicholas School of the Environment, Duke University, Durham, NC, USA, [2]State Key Laboratory of Marine Environmental Science, Xiamen University, Xiamen, FJ, China, [3]Fujian Provincial Key Laboratory of Coastal Ecology and Environmental Studies, Xiamen University, Xiamen, FJ, China, [4]Now at Department of Geosciences, Oberlin College, Oberlin, OH, USA, [5]Marine Chemistry and Geochemistry Department, Woods Hole Oceanographic Institution, Woods Hole, MA, USA, [6]CNRS, Université de Brest, IRD, Ifremer, LEMAR, Plouzané, France

Abstract In this study, we compare mechanistic and empirical approaches to reconstruct the air-sea flux of biological oxygen ($F_{[O_2]_{bio\text{-}as}}$) by parameterizing the physical oxygen saturation anomaly ($\Delta O_{2[phy]}$) in order to separate the biological contribution from total oxygen. The first approach matches $\Delta O_{2[phy]}$ to the monthly climatology of the argon saturation anomaly from a global ocean circulation model's output. The second approach derives $\Delta O_{2[phy]}$ from an iterative mass balance model forced by satellite-based physical drivers of $\Delta O_{2[phy]}$ prior to the sampling day by assuming that air-sea interactions are the dominant factors driving the surface $\Delta O_{2[phy]}$. The final approach leverages the machine-learning technique of Genetic Programming (GP) to search for the functional relationship between $\Delta O_{2[phy]}$ and biophysicochemical parameters. We compile simultaneous measurements of O_2/Ar and O_2 concentration from 14 cruises to train the GP algorithm and test the validity and applicability of our modeled $\Delta O_{2[phy]}$ and $F_{[O_2]_{bio\text{-}as}}$. Among the approaches, the GP approach, which incorporates ship-based measurements and historical records of physical parameters from the reanalysis products, provides the most robust predictions ($R^2 = 0.74$ for $\Delta O_{2[phy]}$ and 0.72 for $F_{[O_2]_{bio\text{-}as}}$; RMSE = 1.4% for $\Delta O_{2[phy]}$ and 7.1 mmol O_2 m^{-2} d^{-1} for $F_{[O_2]_{bio\text{-}as}}$). We use the empirical formulation derived from GP approach to reconstruct regional, inter-annual, and decadal variability of $F_{[O_2]_{bio\text{-}as}}$ based on historical oxygen records. Overall, our study represents a first attempt at deriving $F_{[O_2]_{bio\text{-}as}}$ from snapshot measurements of oxygen, thereby paving the way toward using historical O_2 data and a rapidly growing number of O_2 measurements on autonomous platforms for independent insight into the biological pump.

1. Introduction

Oceans are the largest inventory of actively cycling carbon in the world, accounting for approximately half of global net primary production and sequestering 30% of anthropogenic CO_2 emissions (Field et al., 1998; Friedlingstein et al., 2020; Gruber et al., 2019). The biological transfer of organic matter from the surface to the ocean interior via the biological pump is one of the primary pathways for marine CO_2 uptake and long-term storage (Boyd et al., 2019; Sigman & Boyle, 2000; Volk & Hoffert, 1985). Accurate quantification of the biological pump is a key step toward characterizing the marine carbon cycle and its feedback on future climate change (Ducklow & Doney, 2013).

Net community production (NCP) results from the balance of gross primary production and community respiration. Thus, it reflects the amount of organic matter produced in the upper layer available for export to the deep ocean, thereby constraining the biological pump's potential (Li & Cassar, 2017). The most common approaches to estimate export production and NCP include sediment traps (Betzer et al., 1984; Elskens et al., 2008), ^{234}Th-^{238}U tracer (Buesseler, 1998; Murray et al., 1996), incubation-based NO_3^- incorporation rates (Dugdale & Goering, 1967; Eppley & Peterson, 1979), diel cycles of the microbially mediated oxygen fluxes via light-dark bottle incubation (Serret et al., 2001; Williams & Purdie, 1991), budgeting of biologically important tracers (Huang et al., 2022; Plant et al., 2016; Sarma, 2004), satellite estimates based on remotely sensed properties (Laws et al., 2011; Li & Cassar, 2016; Tilstone et al., 2015), and the dissolved O_2/Ar ratio (Cassar et al., 2009; Craig & Hayward, 1987; Spitzer & Jenkins, 1989) (see further discussion below).

The oxygen saturation anomaly ($\Delta O_{2[total]}$), defined as the percentage departure of the dissolved oxygen concentration from saturation, can be decomposed into abiotic ($\Delta O_{2[phy]}$) and biotic anomalies ($\Delta O_{2[bio]}$). $\Delta O_{2[bio]}$ results from biological generation and consumption of oxygen (NCP) and other processes such as air-sea gas

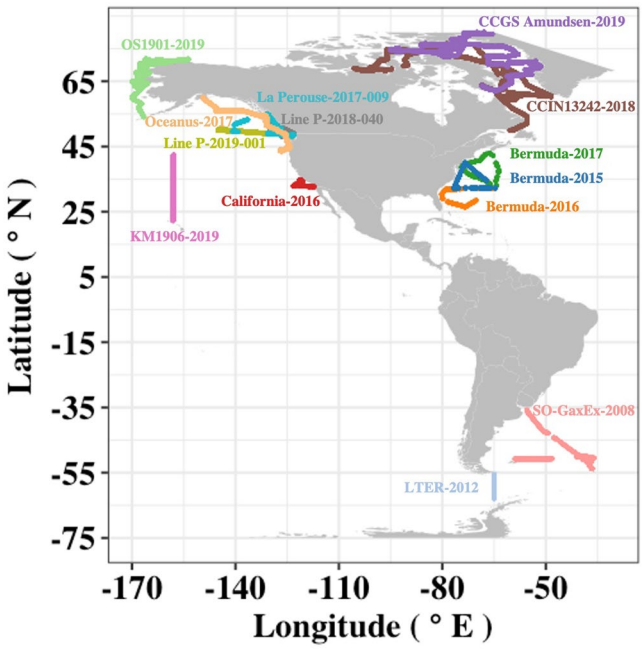

Figure 1. Map of underway concurrent measurements of O_2/Ar and O_2 concentration from 14 cruises used for model training/validation.

exchange of biological oxygen ($F_{[O_2]_{bio\text{-}as}}$) and vertical and horizontal mixing of biological oxygen (Cassar et al., 2014). On seasonal timescales, $F_{[O_2]_{bio\text{-}as}}$ is the primary driver of atmospheric potential oxygen and reflects the overall balance between marine NCP and ventilation (Keeling, 1993; Nevison et al., 2012, 2018). In regions where vertical and horizontal mixing is weak, $F_{[O_2]_{bio\text{-}as}}$ approximates NCP (see details in Section 2.2). $\Delta O_{2[bio]}$ can be estimated from $\Delta O_{2[total]}$ and $\Delta O_{2[phy]}$. In the field, an increasingly used approach to account for $\Delta O_{2[phy]}$ is to concurrently measure the inert gas, Ar, which has similar physical properties as oxygen (Cassar et al., 2009; Craig & Hayward, 1987; Spitzer & Jenkins, 1989). However, most dissolved O_2 measurements are not paired with inert gas measurements. Importantly, the long history and high precision of the dissolved oxygen record in oceanography (Schmidtko et al., 2017) and the recent exponential increase in observations on remote platforms (e.g., profiling floats, moorings, and gliders) (Chai et al., 2020; Claustre et al., 2020) provide a unique opportunity for insight into the spatial and temporal variability of $F_{[O_2]_{bio\text{-}as}}$ and NCP.

In this study, we derive and test empirical and mechanistic algorithms of $\Delta O_{2[phy]}$ with the goal of estimating $\Delta O_{2[bio]}$ from the growing number of surface ocean O_2 observations. The first algorithm adopts the saturation anomaly of Ar predicted from a global ocean circulation model (hereafter called OGCM). The second algorithm derives $\Delta O_{2[phy]}$ using satellite-derived physical drivers (i.e., temperature, wind speed, sea-level pressure) prior to the sampling day to force an iterative air-sea gas exchange model (hereafter called IAGM). The third approach uses the machine-learning approach of Genetic Programming to search for the empirical relationship between $\Delta O_{2[phy]}$ and biophysicochemical parameters (hereafter called GPEM). We assess the models' performance by comparing simulations to field-collected $\Delta O_{2[phy]}$ and $\Delta O_{2[bio]}$ from 14 cruises. This study represents a proof-of-concept effort to reconstruct $F_{[O_2]_{bio\text{-}as}}$ and NCP based on measurements of total oxygen with the long-term objective of mining historical O_2 datasets and a rapidly growing number of O_2 observations on autonomous platforms to better understand oxygen and carbon cycling in the ocean.

2. Methods

2.1. Data Sources

2.1.1. Physical and Biological Variables Used in the Three Models

The monthly climatology of the noble gas saturation anomaly of Ar used in OGCM is from a global ocean circulation model output (http://lod.bco-dmo.org/id/dataset/675575) (Nicholson et al., 2016). The meteorological and biological parameters used in IAGM and GPEM include: daily sea-level air pressure (P_{SLP}), wind speed, relative air humidity, net air-sea heat flux at 2.5° resolution from NCEP/NCAR Reanalysis 1 (https://psl.noaa.gov/data/gridded/data.ncep.reanalysis.html; Kalnay et al., 1996), 8-day average mixed layer depth (MLD) at 0.08° resolution (http://orca.science.oregonstate.edu/1080.by.2160.monthly.hdf.mld125.hycom.php), remotely sensed daily chlorophyll-*a* at 0.08° resolution (https://oceancolor.gsfc.nasa.gov/), and 8-day average net primary production (CbPM, Westberry et al. (2008)) at 0.08° resolution (http://sites.science.oregonstate.edu/ocean.productivity/index.php). The MLD is defined as the depth with 0.125 kg/m^3 density increase relative to the 10 m reference based on the hydrographic data from the HYCOM model simulation (Wallcraft et al., 2008). The change in sea surface temperature (ΔSST_Qnet) driven by atmospheric forcing is computed from remotely sensed net air-sea heat flux (Q_{net}), combined with MLD and seawater heat capacity (C_ρ) (Millero et al., 1973) (Equations S1 and S2 in Supporting Information S1). We back-calculate SST records by subtracting daily ΔSST_Qnet from the ship-board temperature on the sampling date (Stanley et al., 2009).

2.1.2. Underway Concurrent Measurements of O_2/Ar and O_2 for the Model Training and Validation

To evaluate the performance of our three numerical approaches, we compile field measurements of O_2/Ar and O_2 from 14 cruises (Figure 1, Table S1 in Supporting Information S1): two cruises in the Southern Ocean,

SO-GasEx-2008 (https://www.bco-dmo.org/dataset/4059; Hamme et al., 2012), and LTER-2012 (https://zenodo.org/record/5786352; Eveleth et al., 2017), three cruises in the North Atlantic (Bermuda-2017, Bermuda-2016, and Bermuda-2015, https://zenodo.org/record/5786352; Tang et al., 2019; Wang et al., 2018), six cruises in North Pacific, KM1906-2016 (https://zenodo.org/record/4009653#.YmY7WfPMJhE; Juranek et al., 2020), Oceanus-2017, Line P-2019-001, Line P-2018-040 and La Perouse-2017-009 (https://doi.pangaea.de/10.1594/PANGAEA.933345; Izett et al., 2021; R. Izett & Tortell, 2020), California-2016 (https://oceaninformatics.ucsd.edu/datazoo/catalogs/ccelter/datasets/290; Wang et al., 2020), and three Arctic cruises, OS191901-2019 (https://arcticdata.io/catalog/view/doi%3A10.18739/A2HH6C69V), CCGS Amunden-2019 (https://doi.pangaea.de/10.1594/PANGAEA.933345; Izett et al., 2021), and CCIN13242-2018 (https://zenodo.org/record/6124142#.YmheU_PMK3I; Izett et al., 2021). The data near the ice-covered regions from the LTER-2012 cruise are not included because of difficulties in parameterizing the effects of ice dynamics on gas saturation (Cassar et al., 2021; Eveleth et al., 2014).

2.1.3. Global Oxygen Dataset for the Reconstruction of $F_{[O_2]_{bio\text{-}as}}$ and Field Measurements for Comparison

As a proof-of-concept, we leverage global historical oxygen observations and GPEM to extend the limited number of $F_{[O_2]_{bio\text{-}as}}$ observations at the global scale based on the global oxygen dataset. To that end, we combine oxygen observations from the World Ocean Database 2018 (https://www.ncei.noaa.gov/products/world-ocean-database) (Boyer et al., 2018), the Hawaii Ocean Time-Series (HOT, 22.5°N and 158°W, https://hahana.soest.hawaii.edu/hot/), Station Papa (50.0°N, 145.0°W; https://www.waterproperties.ca/linep/publications.php), the Bermuda Atlantic Time-Series Study (BATS, 31.7°N, 64.2°W; http://bats.bios.edu/) and Atlantic Meridional Transect cruises (https://www.amt-uk.org/Cruises). We also compile field estimates based on O_2/Ar ratio measurements as a first-order evaluation of our large-scale projection. Discrete and underway O_2/Ar data include samples collected and measured at HOT by Juranek and Quay (2005) and Quay et al. (2010), at Station Papa by Giesbrecht et al. (2012) and Timmerman et al. (2021) (https://doi.pangaea.de/10.1594/PANGAEA.923370), at BATS by Luz and Barkan (2009), and on two Atlantic Meridional Transect cruises (AMT-16 and AMT-17) by Juranek et al. (2010) (data provided by the first or corresponding author in the studies aforementioned).

2.2. Principle for Estimating $F_{[O_2]_{bio\text{-}as}}$ From Total Oxygen

Following Bushinsky and Emerson (2015), the time rate of change of dissolved O_2 in the mixed layer (MLD × d [O_2] /dt) can be expressed as the sum of the fluxes induced by NCP (mixed layer integrated photosynthesis minus respiration, $J_{[O_2]\text{-NCP}}$), and a set of physical (abiotic) processes including air-sea exchange ($F_{[O_2]\text{-as}}$), vertical mixing at the base of the mixed layer ($F_{[O_2]\text{-v}}$, broadly referring to the vertical processes including entrainment, diapycnal mixing, and wind-stress induced vertical advection), and horizontal advection ($F_{[O_2]\text{-h}}$):

$$\mathrm{MLD}\frac{\mathrm{d}[O_2]}{\mathrm{dt}} = \underbrace{-F_{[O_2]\text{-as}} - F_{[O_2]\text{-v}} - F_{[O_2]\text{-h}}}_{\text{Physical processes}} + J_{[O_2]\text{-NCP}} \quad (1)$$

In our study, we define the increase of oxygen within MLD as positive. The dissolved oxygen concentration in the seawater ([O_2]) can further be decomposed into biological ($[O_2]_{bio}$) and physical (or abiotic) ($[O_2]_{phy}$) components over the residence time of O_2 within the mixed layer (Equation 2):

$$[O_2] = [O_2]_{bio} + [O_2]_{phy} \quad (2)$$

A mass balance equation similar to Equation 1 can be derived specifically for the biological oxygen signal at the ocean surface (Cassar et al., 2014; Equation 3):

$$\begin{aligned}\mathrm{MLD}\frac{\mathrm{d}[O_2]_{bio}}{\mathrm{dt}} &= \mathrm{MLD}\frac{\mathrm{d}[O_2]}{\mathrm{dt}} - \mathrm{MLD}\frac{\mathrm{d}[O_2]_{phy}}{\mathrm{dt}} \\ &= \underbrace{-\left(F_{[O_2]\text{-as}} - F_{[O_2]_{phy}\text{-as}}\right)}_{F_{[O_2]_{bio}\text{-as}}} \underbrace{-\left(F_{[O_2]\text{-v}} - F_{[O_2]_{phy}\text{-v}}\right)}_{F_{[O_2]_{bio}\text{-v}}} \underbrace{-\left(F_{[O_2]\text{-h}} - F_{[O_2]_{phy}\text{-h}}\right)}_{F_{[O_2]_{bio}\text{-h}}} + J_{[O_2]\text{-NCP}}\end{aligned} \quad (3)$$

where the subscripts "bio" and "phy" refer to biological and physical oxygen, respectively. The only common term between Equations 1 and 3 is $J_{O_2\text{-NCP}}$. In other words, the impact of NCP on the total and biological O_2 signals is identical. All the other terms of mixing, air-sea gas exchange, and time-rate of change do not have to be the same for total and biological O_2. This is because the saturation gradients for these properties may not be the same (despite having identical exchange coefficients). For example, the oxygen saturation anomaly below the mixed layer may result from biological activity in the deep chlorophyll maximum or from subsurface heating.

O_2/Ar-based estimates of NCP do not require an assumption of steady-state, representing a weighted average of past NCP (Teeter et al., 2018). For simplicity, we here assume steady-state (i.e., $d[O_2]_{bio}/dt = 0$, Equation 3) can be rearranged with $F_{[O_2]_{bio\text{-as}}}$ reflecting the balance between NCP and vertical and horizontal mixing of biological oxygen:

$$F_{[O_2]_{bio\text{-as}}} = \underbrace{-\left(F_{[O_2]\text{-v}} - F_{[O_2]_{phy\text{-v}}}\right)}_{F_{[O_2]_{bio\text{-v}}}} \underbrace{-\left(F_{[O_2]\text{-h}} - F_{[O_2]_{phy\text{-h}}}\right)}_{F_{[O_2]_{bio\text{-h}}}} + J_{[O_2]\text{-NCP}} \quad (4)$$

$F_{[O_2]_{bio\text{-as}}}$ (the term on the left-hand side) can be parameterized from $\Delta O_{2[total]}$ if $\Delta O_{2[phy]}$ can be accurately estimated or modeled (Equation 5):

$$F_{[O_2]_{bio\text{-as}}} = k_{O_2} \times \left([O_2] - [O_2]_{phy}\right) = k_{O_2} \times \left(\Delta O_{2[total]} - \Delta O_{2[\,phy,\,modeled]}\right) \times [O_2]_{sat} \quad (5)$$

where k_{O_2} is the gas exchange velocity parameterized by wind speed (Wanninkhof, 2014) (with a wind speed history weighting technique, Teeter et al. (2018)), and $[O_2]_{sat}$ is the oxygen concentration at saturation calculated from temperature, salinity, and P_{SLP} (Garcia & Gordon, 1992). When vertical and horizontal mixings are also negligible, $F_{[O_2]_{bio\text{-as}}}$ is a measure of NCP in the mixed layer (Equation 6):

$$F_{[O_2]_{bio\text{-as}}} \approx J_{[O_2]\text{-NCP}} \quad (6)$$

$\Delta O_{2[phy]}$ is often estimated from anomalies in Ar because of their similar solubility and diffusive properties (Craig & Hayward, 1987). Using Ar as a proxy for $\Delta O_{2[phy]}$ introduces minor uncertainties (Eveleth et al., 2014).

2.3. Algorithms to Estimate $\Delta O_{2[phy]}$

2.3.1. OGCM: $\Delta O_{2[phy]}$ Predicted From the Global Ocean Circulation Model

In this algorithm, we adopt the modeled monthly climatology of ΔAr simulations derived from the OGCM model (Nicholson et al., 2016) to represent the $\Delta O_{2[phy]}$. The corresponding ΔAr is extracted by matching the *in situ* record of total oxygen to the closest grid of model output according to the sampling location and date. The modeled ΔAr includes the combined effects of multiple physical processes (i.e., temperature, salinity, P_{SLP}, bubble, and water mass mixing) on the saturation state anomaly using an offline tracer simulation (Khatiwala, 2007; Nicholson et al., 2016). The circulation model used in Nicholson et al. (2016) is based on an ocean state estimate provided by the Estimating the Circulation and Climate of the Ocean (ECCO, version 2) consortium. The ECCO model is forced by adjusting the air-sea fluxes of heat, momentum, and freshwater in the MIT ocean general circulation model. The horizontal resolution of this model is 1° × 1° with 23 vertical levels from 0 to 2,000 m. The air-sea exchange processes (i.e., air-sea gas diffusion and bubble injection) are dictated by applying the air-sea exchange model of Nicholson et al. (2011) to simulate ΔAr. The magnitudes of bubble-mediated flux processes are inversely constrained by a database of deep ocean noble gas and dissolved nitrogen observations (Ne, N_2, Ar, Kr, and Xe). The wind speed and P_{SLP} used to force the air-gas exchange model are taken from the 6-hourly CORE v2 data set. The ΔAr output presented in this study represents monthly climatology over the 1992–2004 period.

2.3.2. IAGM: $\Delta O_{2[phy]}$ Predicted From an Iterative Air-Sea Gas Model

In the second approach, we develop a mechanistic semi-analytical model to estimate the $\Delta O_{2[phy]}$. Studies suggest that air-sea gas exchange is generally the dominant process controlling the surface inert gas saturation in the open ocean and that other physical processes (e.g., vertical mixing and horizontal advection) are of second-order impor-

tance (Bushinsky & Emerson, 2015; Huang et al., 2018; Nicholson et al., 2011). As a first approximation, we assume that the effects of other physical processes ($F_{[O_2]_{phy\text{-}h}}$ and $F_{[O_2]_{phy\text{-}v}}$) on $\Delta O_{2[phy]}$ are negligible (Equation 7).

$$MLD\frac{d\,[O_2]_{phy}}{dt} \approx -F_{[O_2]_{phy\text{-}as}} \tag{7}$$

In our model, $F_{[O_2]_{phy\text{-}as}}$ (and $\Delta O_{2[phy]}$) are determined by the P_{SLP} and temperature effects on solubility, bubble, and diffusive gas exchange processes. To compute daily air-sea gas exchange fluxes, we adopt the air-sea gas exchange model developed by Liang et al. (2013) with the modifications to the bubble effect suggested by Emerson et al. (2019). This air-sea gas model explicitly includes the bubble-mediated gas flux.

The model is run iteratively with 1-day time steps and forced by the direct history of daily wind speed, P_{SLP} with a water vapor correction (Weiss & Price, 1980), and temperature prior to the observation at each time step obtained from the reanalysis model (NCEP Reanalysis-I). We assume unchanged salinity throughout the model run duration, which should not have a large impact as the salinity influence on O_2 solubility (away from ice and river outflows) is small (Hamme & Emerson, 2004). At each time step, the coefficients of the air-sea gas model and oxygen saturation are adjusted according to the corresponding physical parameters of that day. We correct for the effect of historical changes in P_{SLP} on the O_2 saturation (ΔO_2) by multiplying the saturation by the ratio of the P_{SLP} to standard pressure (i.e., $\Delta O_2 = O_2/O_{2[sat]} \times \left([P_{SLP} - P_{H_2O}]/[1,013.25 - P_{H_2O}]\right)$, where P_{H_2O} is the water vapor and $O_{2[sat]}$ is the oxygen concentration at the saturation sate under the given temperature and salinity condition) (Izett & Tortell, 2021).

The iterative mass balance model is initialized assuming equilibrium conditions ($\Delta O_{2[phy]}$ at 0%), at the surface temperature, salinity, and P_{SLP} we set up at the first-time step. The run duration at each sampling location is adjusted to the corresponding 4.6 residence time (representing a ~99% oxygen ventilation, approximately 20–150 days depending on the wind speed and thickness of the mixed layer). O_2 saturation anomaly at the end of the model run is extracted as the state of $\Delta O_{2[phy]}$, which is then used to isolate $\Delta O_{2[bio]}$ from the field observation of $\Delta O_{2[total]}$ (Equation 5) for the calculation of $F_{[O_2]_{bio\text{-}as}}$. We compare this approach to the one in which we set the initial equilibrium conditions as the monthly Ar climatology predicted from OGCM (which is considered to provide a metric closer to the local steady-state, see the following discussion). These attempts yielded limited improvements in model accuracy.

2.3.3. GPEM: $\Delta O_{2[phy]}$ Predicted From the Empirical Model Derived From Genetic Programming

The third approach is to leverage the machine-learning technique of Genetic Programming (GP) to search for the empirical relationship between $\Delta O_{2[phy]}$ and biophysicochemical variables. Under some circumstances, the GP equation can identify the underpinning mechanisms controlling the $\Delta O_{2[phy]}$. Briefly, GP is a machine learning algorithm based on evolutionary computation and can be used to conduct symbolic regression (Koza, 1994). Akin to biological evolution, evolutionary algorithms randomly mutate the offspring during the model training, and only the offspring with the highest fitness for a given complexity are reproduced.

To develop the GPEM, we select eight cruises for training (Bermuda-2016, Bermuda-2015, La Perouse-2017-009, LTER-2012, Line P-2018-040, Ocean-2017, CCIN1342-2018, and CCGS Aumudesn-2019) (n = 1,208) and the remaining six cruises as an independent validation dataset (Bermuda-2017, OS1901-2019, KM1906-2016, California-2016, SO-GaxEx-2008, and Line P-2019-001) (n = 1,352). The training and validation datasets both encompass a wide spectrum of ocean provinces (e.g., subtropical ocean, subarctic ocean, Arctic, and coastal regions) and ensure the generalizability of the model training and validation. We select a suite of environmental predictors which might be directly or indirectly related to the observed $\Delta O_{2[phy]}$, including the sampling date and location, field measured variables ($\Delta O_{2[total]}$, O_2, sea surface temperature, and salinity), historical records of physical and biological parameters from satellite observations and reanalysis models (e.g., MLD, sea surface temperature, wind speed, P_{SLP}, chlorophyll-a, and net primary production). The detailed description of the predictors is summarized in Table S2 in Supporting Information S1. We include all possible predictors into the model training and allow the machine to identify the most reliable predictors.

GP generates a set of candidate solutions with model accuracy generally increasing with complexity (Table S3 in Supporting Information S1). Selection of a solution is somewhat arbitrary, reflecting a trade-off between balancing model accuracy and complexity. For our GPEM, we choose the equation with a complexity level of 8 because a limited improvement in model accuracy results from greater complexity (Equation 8):

Table 1
Summary of Field Observations/Estimates Used for Model Training/Validation

	$\Delta O_{2[phy]}$	$\Delta O_{2[bio]}$	$F_{[O_2]_{bio\text{-}as}}$
Field observation	ΔAr	$(1+\Delta Ar)\times(\Delta O_2/Ar)$	$k_{O_2}\times(\Delta O_2/Ar)\times[O_2]_{sat}$
Model	$\Delta O_{2[phy]}$	$\Delta O_{2[total]}-\Delta O_{2[modeled,phy]}$	$k_{O_2}\times\left(\Delta O_{2[total]}-\Delta O_{2[modeled,phy]}\right)\times[O_2]_{sat}$

Note. $\Delta O_{2[total]}$: total (observed) oxygen saturation anomaly with the correction for sea-level pressure and water vapor; $\Delta O_{2[phy]}$: physical oxygen saturation anomaly; $\Delta O_{2[bio]:}$ biological oxygen saturation anomaly; $F_{[O_2]_{bio\text{-}as}}$: air-sea gas flux of biological oxygen; ΔAr: saturation anomaly of Argon; $[O_2]_{sat}$: oxygen concentration at the saturation with the correction for sea-level pressure and water vapor; and k_{O_2}: gas exchange velocity.

$$\Delta O_{2[phy]} = 73.1 + 0.39\times\Delta O_{2[total]\_in\ situ} + 0.048\times SST_{in\_situ} - 7.27\times10^{-2}\times P_{SLP\_in\ situ} + 8.11\times\overline{\Delta SST} \quad (8)$$

where SST_{in_situ} (°C) is the underway measurement of sea surface temperature, $P_{SLP\_in\ situ}$ (mbar) is the contemporaneous sea-level pressure on the sampling date, and $\Delta O_{2[total]\_in\ situ}$ (%) is the ship-board measured total oxygen anomaly with the correction for $P_{SLP\_in\ situ}$ and water vapor ($\Delta O_{2[total]\_in\ situ} = O_2/O_{2[sat]}\times\left([P_{SLP\_in\ situ}-P_{H_2O}]/[1,013.25-P_{H_2O}]\right)$). $\overline{\Delta SST}$ (°C d^{-1}) represents the linear slope of the historical SST change calculated as the difference in the end-member values between the sampling date (SST_{day_0}) and the date prior to the sampling date corresponding to the residence time of oxygen within MLD (SST_{day_-n}), divided by the residence time in days ($\overline{\Delta SST} = (SST_{day\_0}-SST_{day\_-n})/n$, where n is the day length of residence time of oxygen within MLD). Repeated reconstructions of the training dataset result in equations with equivalent performance and similar predictors.

2.4. Model Validation by Field Measurements

Fourteen cruises with simultaneous measurements of total oxygen concentration and O_2/Ar ratio are used for model validation (Figure 1). The continuous underway measurements are averaged into daily values with 0.5° × 0.5° resolution to reduce spatial and temporal autocorrelation between observations.

The approaches to calculate $\Delta O_{2[phy]}$, $\Delta O_{2[bio]}$, and $F_{[O_2]_{bio\text{-}as}}$ from field observations and model outputs are summarized in Table 1. The *in situ* measurement of ΔAr can be calculated from the measured $\Delta(O_2/Ar)$ via EIMS and the $\Delta O_{2[total]}$ (with the correction for P_{SLP} and water vapor) measured by the optode (Equation 9). The detailed derivation of Equation 9 is described in Eveleth et al. (2017):

$$\Delta Ar = \frac{\Delta O_{2[total]}+1}{(\Delta(O_2/Ar)+1)} - 1 \quad (9)$$

$\Delta O_{2[bio]}$ is derived from field measurements of $\Delta(O_2/Ar)$ and ΔAr following Equation 10:

$$\Delta O_{2[bio]} = \frac{[Ar]}{[Ar]_{sat}}\Delta(O_2/Ar) = (1+\Delta Ar)\,\Delta(O_2/Ar) \quad (10)$$

$\Delta O_{2[bio]}$ is used to calculate the *in situ* $F_{[O_2]_{bio\text{-}as}}$ according to the equations presented in Table 1.

2.5. Statistical Analysis

To evaluate the predictive skills of the algorithms, we calculate the coefficient of determination (R^2) and root mean square error (RMSE) for pairwise *in situ* observations versus model simulations for the test dataset. The significance is satisfied if the type I error rate (p) is less than 0.05. All the figures and statistical analyses are performed in R (R Core Team, 2014).

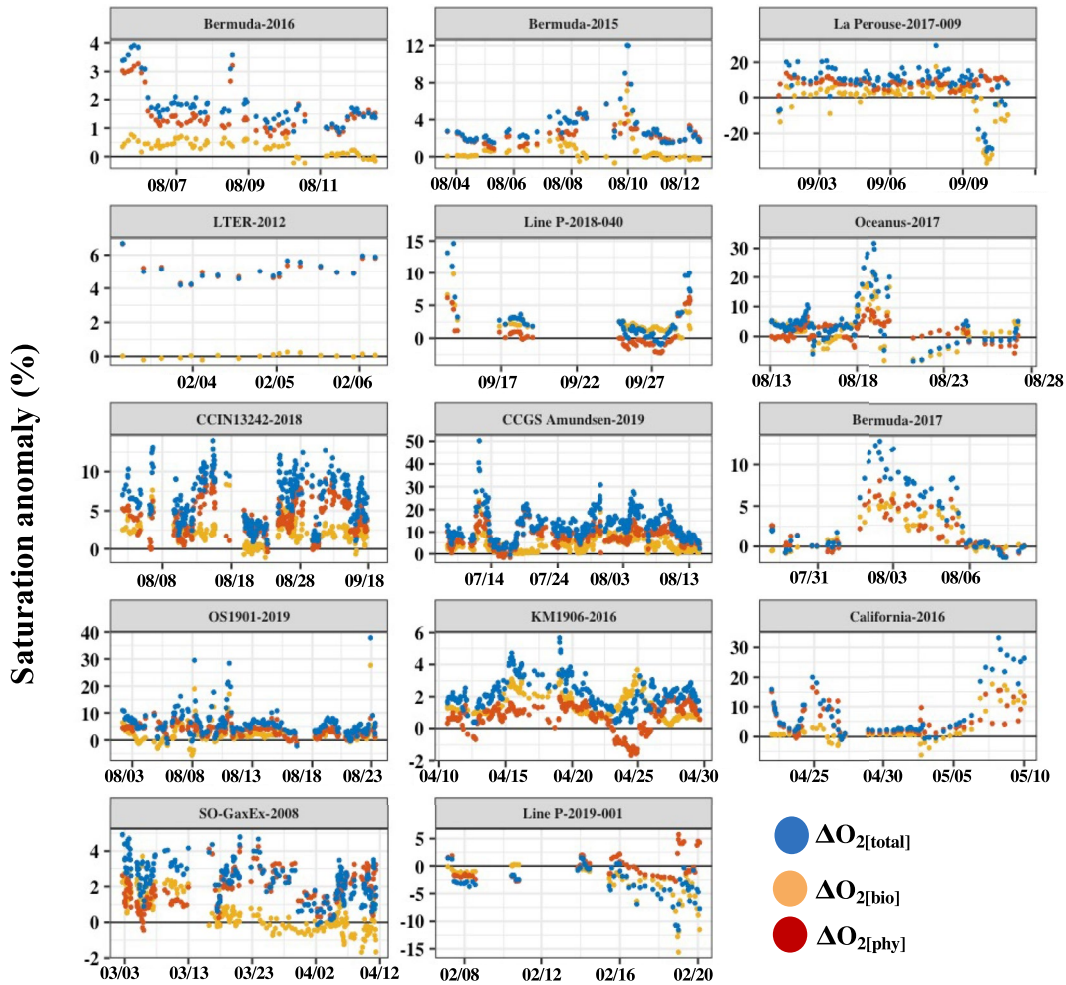

Figure 2. Underway measurements of the total, physical, and biological oxygen saturation anomalies ($\Delta O_{2[total]}$, $\Delta O_{2[phy]}$, and $\Delta O_{2[bio]}$, respectively) on the 14 cruises shown in Figure 1. Note: $\Delta O_{2[total]}$ is derived from the optode oxygen and underway temperature and salinity measurements (with the correction for sea-level pressure and water vapor). $\Delta O_{2[phy]}$ and $\Delta O_{2[bio]}$ are calculated from the *in situ* O_2/Ar measurements and $\Delta O_{2[total]}$ (Equations 9 and 10).

3. Results and Discussion

3.1. *In Situ* Measurements of $\Delta O_{2[total]}$, $\Delta O_{2[phy]}$, and $\Delta O_{2[bio]}$

$\Delta O_{2[total]}$, $\Delta O_{2[phy]}$, and $\Delta O_{2[bio]}$, and their relations for the 14 cruises are shown in Figures 2 and 3. $\Delta O_{2[total]}$ exhibits substantial variability ranging between −40% and 45%. The dominating factors controlling $\Delta O_{2[total]}$ vary. At low $\Delta O_{2[total]}$, $\Delta O_{2[total]}$, and $\Delta O_{2[bio]}$ converge onto the identity line (Figure 3a), indicating that biological processes are the main factor driving low $\Delta O_{2[total]}$ in our pooled dataset. The negative $\Delta O_{2[bio]}$ observed might reflect heterotrophy (Hamme et al., 2012) or vertical mixing of subsurface oxygen-depleted water (e.g., coastal North Pacific during Line P-2019-001 and La Peouse-2017-009 expeditions) (Izett et al., 2018; Wang et al., 2020). Approximately 75% of $\Delta O_{2[bio]}$ is positive, suggesting a prevailing autotrophic state (i.e., gross primary production exceeding the community respiration). In contrast, high $\Delta O_{2[total]}$ is mainly associated with high $\Delta O_{2[phy]}$ (Figure 3b). Approximately 80% of $\Delta O_{2[phy]}$ is in the range between −4% and 6%, falling within the range of previous open ocean estimates (Eveleth et al., 2014, 2017). This is also comparable with the global range (from −4 to 8%) of direct measurement of surface ΔAr synthesized by Hamme et al. (2019). The extremely high $\Delta O_{2[phy]}$ (i.e., >10% in the Arctic region measured during CCGS Amundsen-2019 expedition) likely results from the combined effect of the artificially induced bubbles in the ship underway lines (Juranek et al., 2010; Izett et al., 2021) and rapid heating event prior to the cruises (Figure S1 in Supporting Information S1).

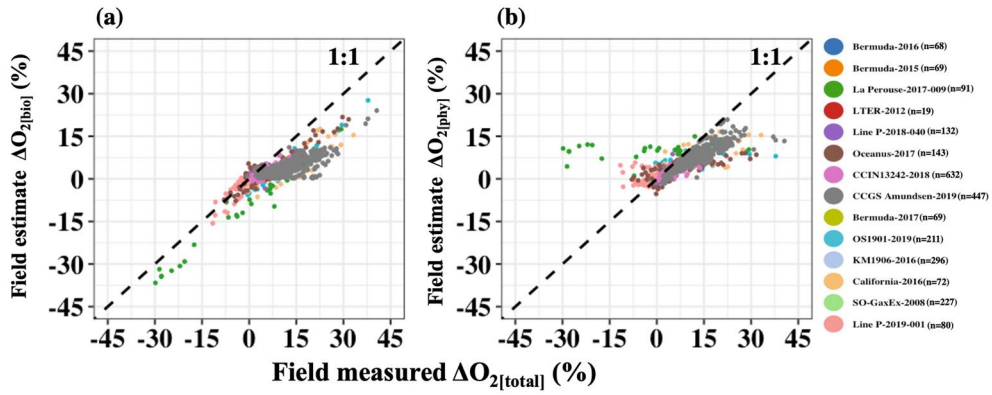

Figure 3. Scatter plot of *in situ* observations/estimates of total oxygen saturation anomaly ($\Delta O_{2[total]}$) with (a) biological oxygen saturation anomaly ($\Delta O_{2[bio]}$) and (b) physical ($\Delta O_{2[phy]}$) for the pooled dataset of 14 cruises. Note: $\Delta O_{2[total]}$ is derived from the optode oxygen and underway temperature and salinity measurements, with the correction for sea-level pressure and water vapor. $\Delta O_{2[phy]}$ and $\Delta O_{2[bio]}$ are calculated from the *in situ* O_2/Ar measurements and $\Delta O_{2[total]}$ (Equations 9 and 10).

The factors controlling the biological and physical anomalies are mostly independent, and thereby their relative intensity ultimately determines their respective contributions (Figures 2 and 3). We observe a close coupling between the $\Delta O_{2[bio]}$ and $\Delta O_{2[total]}$ in the region of the western Atlantic during the year 2017 (Bermuda-2017 expedition), California Current System (California-2016 expedition), central North Pacific (KM1906-2016 expedition). During these cruises, the impact of the biological and physical processes on $\Delta O_{2[total]}$ is comparable. In contrast, $\Delta O_{2[bio]}$ in the Southern Ocean (LTER-2012 and SoGasEx-2012 cruises) and subtropical western Atlantic (Bermuda-2016 cruise) are relatively low, typically less than 2%, and $\Delta O_{2[phy]}$ is a dominating factor governing $\Delta O_{2[total]}$ variability.

3.2. Comparison of Model Simulations to the Field Measurements

A comparison of field and modeled estimates of $\Delta O_{2[phy]}$ for the 14 cruises are presented in Figures 4 and 5a–5c. In principle, OGCM more comprehensively incorporates contributions of physical processes on gas supersaturation such as water mass mixing, entrainment, and advection under the framework of the global circulation model (Nicholson et al., 2016). In contrast, IAGM only accounts for the effect of air-sea transfer on the physical supersaturation. However, the global ocean circulation output is a monthly climatology at a one-degree resolution. Not accounting for the important influence of synoptic events smooths $\Delta O_{2[phy]}$ (Figure 4). Thereby, the model output of $\Delta O_{2[phy]}$ from Nicholson et al. (2016) tends to suggest a saturation signal close to the local steady-state. By accounting for the history of physical drivers prior to the sampling day, IAGM better captures the broad variability of measured $\Delta O_{2[phy]}$ on cruises where rapid changes in SST prior to the sampling day were observed (i.e., Bermuda-2017, Bermuda-2016, KM1906-2016, and LTER-2012 expeditions, Figure 4 and Figure S1 in Supporting Information S1). However, the IAGM model shows limited improvement on the prediction accuracy of $\Delta O_{2[phy]}$ for the pooled dataset ($R^2 = 0.19$, RMSE = 4.5%) compared to OGCM ($R^2 = 0.22$, RMSE = 4.2%, Figures 5a and 5b, Table 2) because of substantial uncertainties in the low $\Delta O_{2[phy]}$ range (0%–3%). The errors may, in part, reflect limitations of the model with poorly constrained contributions and parameterization of air-sea gas fluxes (Emerson et al., 2019; Liang et al., 2017), model initiation $\Delta O_{2[phy]}$ (prior set to 0% in our study), uncertainties in satellite-derived variables, and omitting the vertical mixing terms in IAGM.

GPEM captures the variability relatively well in field estimates of $\Delta O_{2[phy]}$ from the six validation cruises (Figure 4), representing a significant improvement in model performance compared to the other two models ($R^2 = 0.74$, RMSE = 1.4%, Figure 5c, Table 2). The formulation generated by GP incorporates shipboard measurements of SST, $\Delta O_{2[total]}$ with the correction for P_{SLP} and water vapor ($\Delta O_2 = O_2/O_{2[sat]} \times \left([P_{SLP} - P_{H_2O}]/[1,013.25 - P_{H_2O}]\right)$), simultaneous P_{SLP}, and temperature change over the residence time of O_2 within the MLD (Equation 8). Based on a sensitivity analysis and spatiotemporal variability of each predictor in the ocean (Table S4 and Figure S2 in Supporting Information S1), $\Delta O_{2[total]}$ ranks as the most important factor in predicting $\Delta O_{2[phy]}$ in the GEPM. It is a not surprising result because $\Delta O_{2[total]}$ reflects multiple processes (Figure 3). As shown in the pooled dataset (Figure 3b), $\Delta O_{2[total]}$ and $\Delta O_{2[phy]}$ are highly correlated but

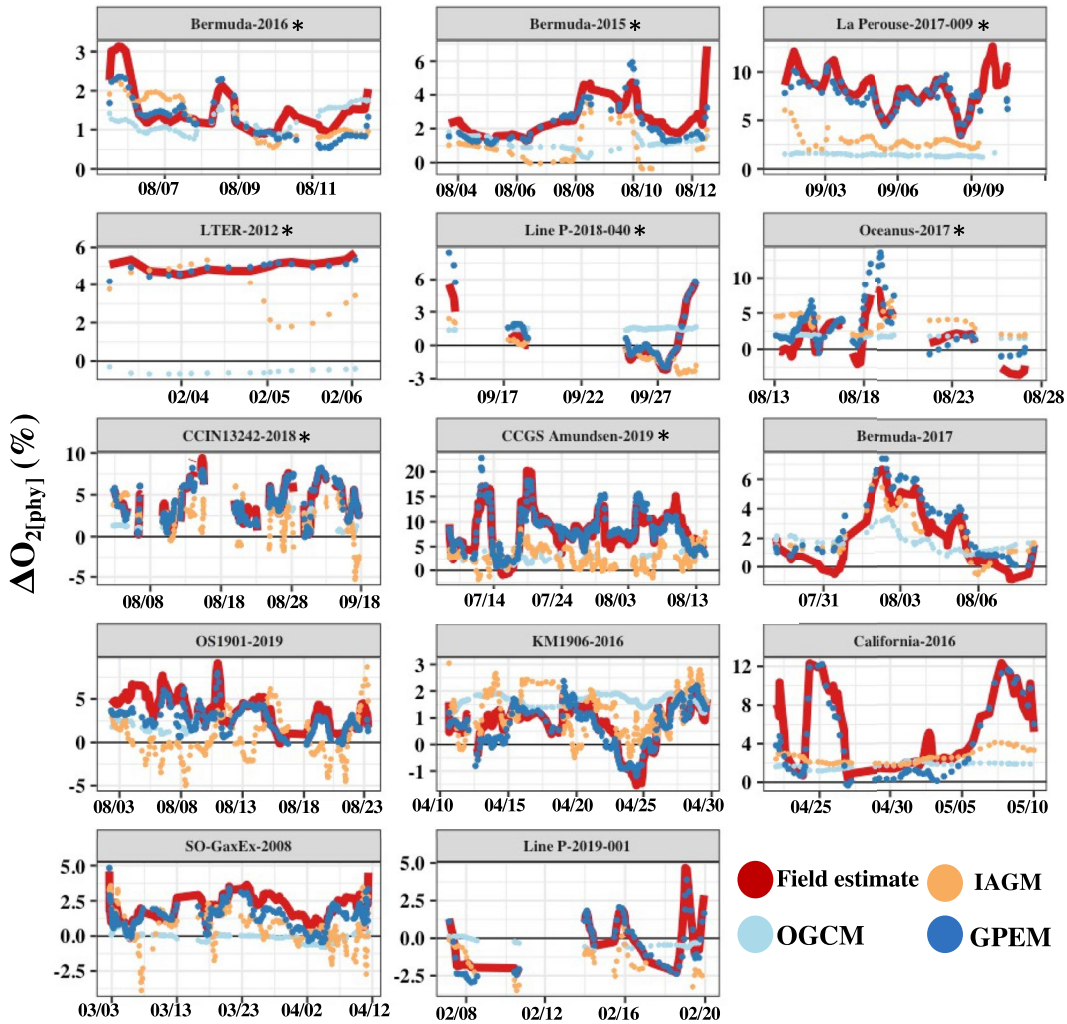

Figure 4. Comparison of model predictions to *in situ* measurements of physical oxygen saturation anomaly ($\Delta O_{2[phy]}$) on the 14 cruises. The cruises labeled with stars refer to the cruises used to train the GPEM algorithm (empirical model derived from Genetic Programming). A 5-point running average was applied to the field estimates. Note: field estimates of $\Delta O_{2[phy]}$ are derived from the in situ O_2/Ar measurement and $\Delta O_{2[total]}$ (Equation 9). OGCM: $\Delta O_{2[phy]}$ predicted from the global ocean circulation model. IAGM: $\Delta O_{2[phy]}$ predicted from an iterative O_2 air-sea gas model.

deviate from the 1:1 line. The role of other physical predictors assimilated in the empirical algorithm is likely to simulate the regionally or temporally dependent offset, allowing better predictions of $\Delta O_{2[phy]}$ from $\Delta O_{2[total]}$. Note that $\Delta O_{2[total]}$ shown herein is a term already incorporating the impact of SLP on the $\Delta O_{2[phy]}$ (by directly altering the oxygen concentration at the saturation, Eveleth et al. (2014)). Interestingly, P_{SLP} is a predictor selected by the GPEM and ranks as a secondary importance factor (Table S4 in Supporting Information S1), suggesting that the GPEM compensates for an incomplete P_{SLP} correction. The importance of SST and SST_{in_situ} are almost equal in GEPM, and less important than $\Delta O_{2[total]}$ and P_{SLP} (Table S4 in Supporting Information S1). In line with the results from the IAGM simulations, rapid temperature changes can be a strong driver of the physical oxygen saturation anomaly in some circumstances. Biological parameters and wind speed were not selected as important predictors, most likely because they are already captured by $\Delta O_{2[total]}$. Uncertainties in these products could also mask their relationship with $\Delta O_{2[phy].}$ We also note that statistical inferences from the equation should be interpreted with caution as GP is predictive, not explanatory.

As expected, when a particular model under-(over-) estimates $\Delta O_{2[phy]}$, the modeled $F_{[O_2]_{bio\text{-}as}}$ shows positive (negative) biases. The OCGM and IGAM do not improve on $F_{[O_2]_{bio\text{-}as}}$ predictions ($R^2 = 0.21$, RMSE = 21 mmol O_2 m^{-2} d^{-1} for OGCM; R^2 = 0.27 RMSE = 18 mmol O_2 m^{-2} d^{-1} for IAGM, Figures 5 and 6, Table 2)

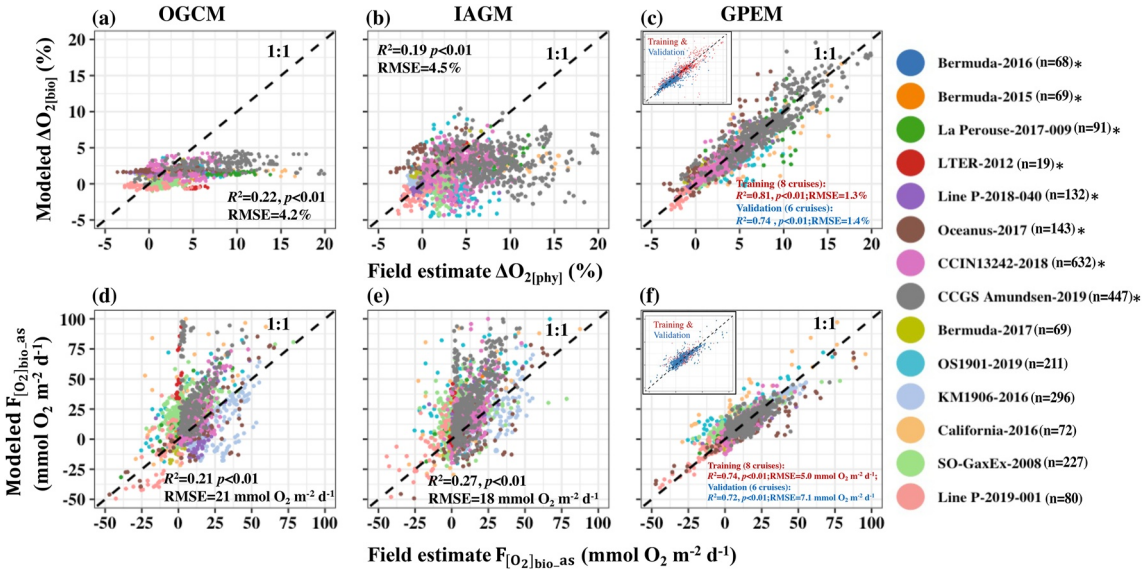

Figure 5. Comparison of model predictions versus *in situ* estimates of (a–c) physical oxygen saturation anomaly ($\Delta O_{2[phy]}$) and (d–f) air-sea biological flux ($F_{[O_2]_{bio\text{-}as}}$) for the pooled dataset. The cruises labeled with stars refer to cruises used to train the GPEM (empirical model derived from Genetic Programming). OGCM: global ocean circulation model. IAGM: iterative O_2 air-sea gas model. Note: field estimates of $\Delta O_{2[phy]}$ are derived from the *in situ* O_2/Ar measurement and $\Delta O_{2[total]}$ (Equation 9).

compared to a model which assumes a constant $\Delta O_{2[phy]}$ of 2.5% (median value of pooled $\Delta O_{2[phy]}$) ($R^2 = 0.18$ RMSE = 20 mmol O_2 m^{-2} d^{-1}). $F_{[O_2]_{bio\text{-}as}}$ derived from GPEM captures the broad spatial variability (Figure 6) in the six validation cruises, and the slopes of simulations versus observations converge onto the identity line (Figures 5d–5f). In regions where vertical mixing is negligible, $F_{[O_2]_{bio\text{-}as}}$ should reflect NCP. Overall, the performance of GPEM ($R^2 = 0.72$, RMSE = 7.1 mmol O_2 m^{-2} d^{-1}, Table 2) is comparable to other NCP models such

Table 2
Prediction Skills of the Three Algorithms Used in This Study to Reconstruct Air-Sea Gas Flux of Biological Oxygen ($F_{[O_2]_{bio\text{-}as}}$) Based on Observations of the Total Oxygen Anomaly

Algorithm	Descriptions	$\Delta O_{2[phy]}$ (n = 2,560)	$F_{[O_2]_{bio\text{-}as}}$ (n = 2,560)
Measured	Underway measurements of O_2/Ar and O_2 concentration	Q_1: 1.2%; Q_2: 2.8%; Q_3: 6.1%	Q_1: 2.1 mmol O_2 m^{-2} d^{-1}; Q_2: 6.8 mmol O_2 m^{-2} d^{-1}; Q_3: 14.9 mmol O_2 m^{-2} d^{-1}
OGCM	The monthly climatology of ΔAr from the global ocean circulation prediction used for $\Delta O_{2[phy]}$	$R^2 = 0.22$, $p < 0.01$; RMSE = 4.2%; Q_1: 0.94%; Q_2: 1.5%; Q_3: 4.5%	$R^2 = 0.21$ $p < 0.01$; RMSE = 21 mmol O_2 m^{-2} d^{-1}; Q_1: 2.0 mmol O_2 m^{-2} d^{-1}; Q_2: 13.1 mmol O_2 m^{-2} d^{-1}; Q_3: 29.1 mmol O_2 m^{-2} d^{-1}
IAGM	$\Delta O_{2[phy]}$ derived from an iterative air-sea gas exchange model	$R^2 = 0.19$, $p < 0.01$; RMSE = 4.5% Q_1: 0.31%; Q_2: 1.64%; Q_3: 2.92%	$R^2 = 0.27$ $p < 0.01$; RMSE = 18 mmol O_2 m^{-2} d^{-1}; Q_1: 4.1 mmol O_2 m^{-2} d^{-1}; Q_2: 15.2 mmol O_2 m^{-2} d^{-1}; Q_3: 29.2 mmol O_2 m^{-2} d^{-1}
GPEM	Empirical equation derived by Genetic Programming	Training dataset (n = 1,208): $R^2 = 0.81$, $p < 0.01$; RMSE = 1.3% Q_1: 2.1%; Q_2: 4.9%; Q_3: 7.7% Validation (n = 1,352): $R^2 = 0.74$ $p < 0.01$; RMSE = 1.4% Q_1: 0.48%; Q_2: 1.42%; Q_3: 2.25%	Training dataset (n = 1,208): $R^2 = 0.74$, $p < 0.01$; RMSE = 5 mmol O_2 m^{-2} d^{-1}; Q_1: 4.1 mmol O_2 m^{-2} d^{-1}; Q_2: 8.5 mmol O_2 m^{-2} d^{-1}; Q_3: 15 mmol O_2 m^{-2} d^{-1} Validation (n = 1,352): $R^2 = 0.72$, $p < 0.01$; RMSE = 7.1 mmol O_2 m^{-2} d^{-1}; Q_1: 4.1 mmol O_2 m^{-2} d^{-1}; Q_2: 13.2 mmol O_2 m^{-2} d^{-1}; Q_3: 20.2 mmol O_2 m^{-2} d^{-1}

Note. Q_1, Q_2, and Q_3 indicate the 25%, 50%, and 75% quartiles of the pooled dataset, respectively. OGCM: global ocean circulation model. IAGM: iterative O_2 air-sea gas exchange model; GPEM: empirical model derived by Genetic Programming.

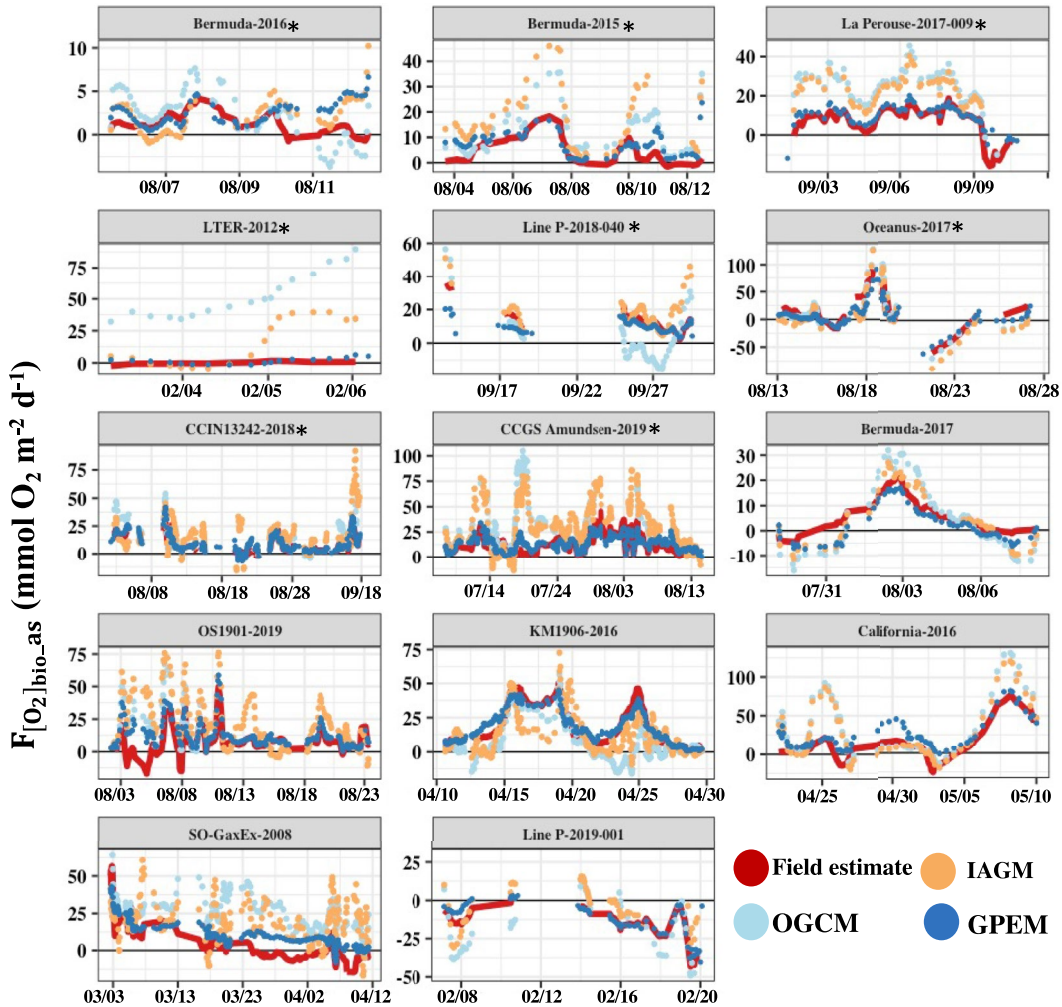

Figure 6. Comparison of model predictions versus *in situ* estimates of the air-sea gas flux of biological oxygen ($F_{[O_2]_{bio\text{-}as}}$). A 5-point running average was applied to the field estimates. The cruises labeled with stars refer to the cruises used to train the GPEM (empirical model derived from Genetic Programming). OGCM: global ocean circulation model. IAGM: iterative O_2 air-sea gas model.

as statistical models based on light-dark bottle incubation (R^2 = 0.61, RMSE = 26 mmol O_2 m^{-2} d^{-1}) (Tilstone et al., 2015) and machine-learning algorithms based on O_2/Ar observations (R^2 = 0.78, RMSE = 2.1 mmol O_2 m^{-2} d^{-1}) (Li & Cassar, 2016).

3.3. Testing the Feasibility of Reconstructing Broad-Scale $F_{[O_2]_{bio\text{-}as}}$ Patterns From Historical Oxygen Observations

As a proof-of-concept, we leverage global historical oxygen observations and the GPEM model to extend the limited number of $F_{[O_2]_{bio\text{-}as}}$ observations at the global scale (Figures 7 and 8). The general agreement between the model simulations and observations is further supported by snapshot O_2/Ar observations at three ocean time-series observation stations (HOT, BATS, and Papa) and on two Atlantic Meridional Transects cruises (AMT-16 and AMT-17) (Figure 7). However, while the general patterns of $F_{[O_2]_{bio\text{-}as}}$ are captured (R^2 = 0.43, $p < 0.05$, RMSE = 8.1 mmol O_2 m^{-2} d^{-1} for the pooled dataset shown in Figure 7), an offset is sometimes present (e.g., AMT-16 and AMT-17).

Our global projection (Figure 8) provides an independent constraint on $F_{[O_2]_{bio\text{-}as}}$ and the drivers of variability in atmospheric potential oxygen. The annual integrated $F_{[O_2]_{bio\text{-}as}}$ are −1.15 mol C m^{-2} yr^{-1} at 50°–70°N,

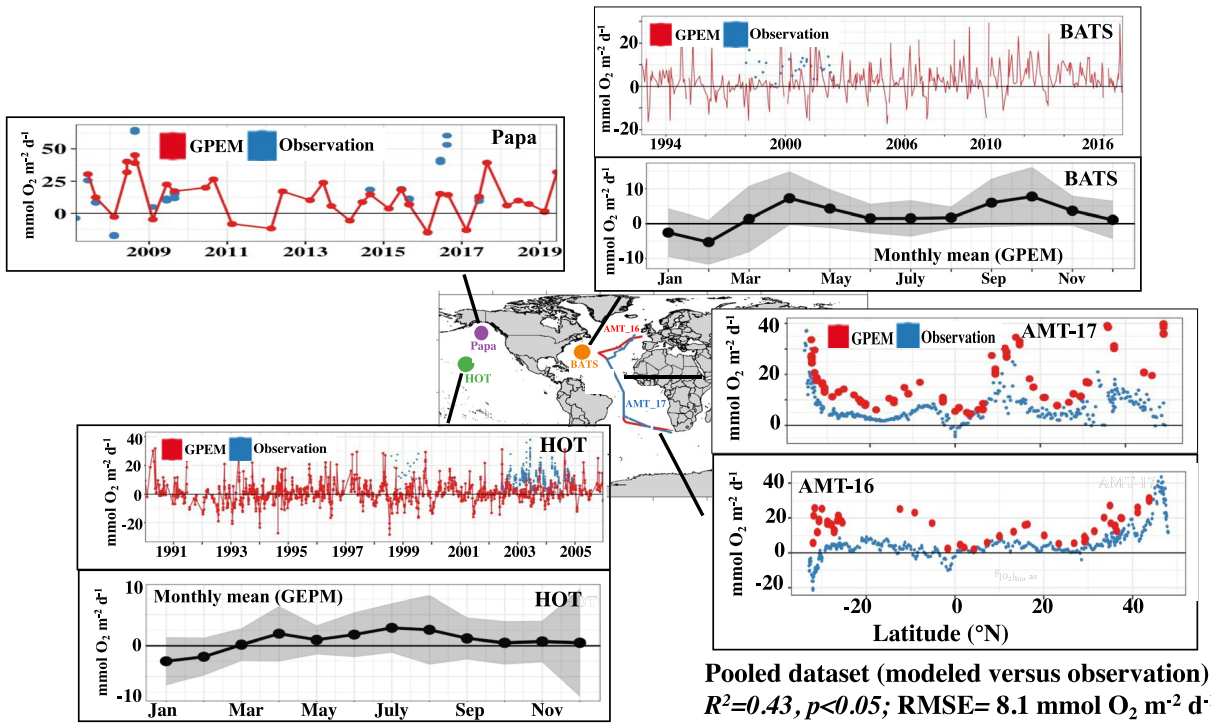

Figure 7. Air-sea gas flux of biological oxygen ($F_{[O_2]_{bio\text{-}as}}$) at three ocean time-series stations (HOT, BATS and Papa) and on two Atlantic Meridional Transects cruises (AMT-16 and AMT-17). The red and blue dots represent estimates derived from our GPEM (empirical model derived from Genetic Programming) and field measurement of O_2/Ar, respectively.

1.3 mol C m^{-2} yr^{-1} at 30°–50°N, 0.8 mol C m^{-2} yr^{-1} at 10°–30°N, 0.01 mol C m^{-2} yr^{-1} at −10°S −10°N, 0.1 mol C m^{-2} yr^{-1} at 10°–30°S, 0.67 mol C m^{-2} yr^{-1} at 30°–50°S and −0.23 mol C m^{-2} yr^{-1} at 30°–50°S (C:O ratio = 1.4, Laws (1991)). In the high latitude, our projected $F_{[O_2]_{bio\text{-}as}}$ displays a more pronounced seasonality, shifting between positive and negative values. $F_{[O_2]_{bio\text{-}as}}$ reflects the overall balance between NCP and ventilation of biological oxygen and thus is not expected to equal NCP in regions with active upwelling (i.e., parts of the Southern Ocean, Cassar et al. (2014); Jonsson et al. (2013), and equatorial ocean, (Wyrtki, 1981)) and strong entrainment process (i.e., subarctic northern Atlantic, Tandon and Zahariev (2001)). It also should be noted that the uneven distribution of oxygen data (i.e., fewer data in the Pacific than Atlantic and during winters, Figure 8a) can lead to biases in latitudinal $F_{[O_2]_{bio\text{-}as}}$ band projections. Overall, global projection implemented herein represents a preliminary effort.

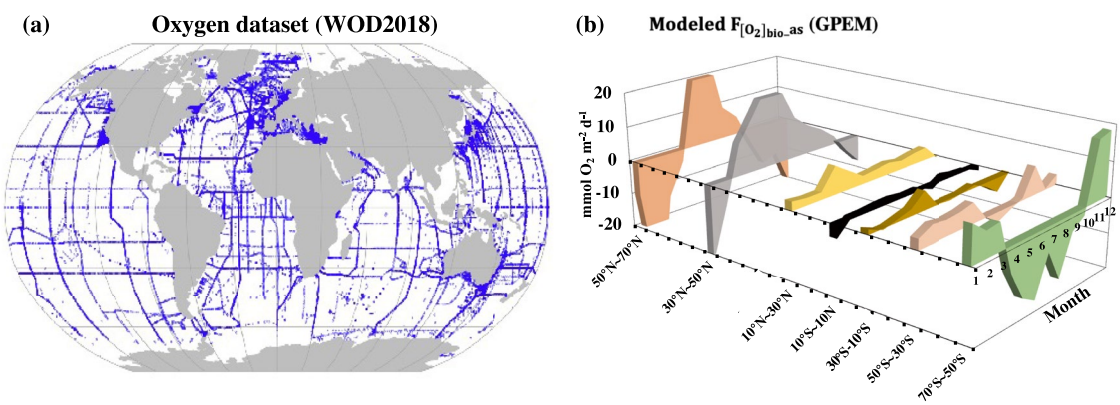

Figure 8. (a) Global distribution of oxygen observations from the World Ocean Database 2018 (WOD2018) and (b) monthly climatology of our GPEM (empirical model derived from Genetic Programming) projected air-sea biological O_2 flux ($F_{[O_2]_{bio\text{-}as}}$) at various latitudinal bands based on the oxygen measurements from Word Ocean Database 2018.

4. Summary and Next Steps

Overall, our study represents a first attempt at reconstructing $F_{[O_2]_{bio\text{-}as}}$ and NCP from global measurements of total oxygen and paves the way toward fully utilizing the historical O_2 data and a rapidly growing number of autonomous measurements in constraining the biological pump. This study uses empirical and mechanistic approaches to parameterize $\Delta O_{2[phy]}$. Model performance is evaluated by comparison against observations collected on 14 cruises across several ocean basins. The third algorithm, which is an empirical function incorporating field-measured properties and the history of physical parameters prior to the sampling day, provides the most reliable estimates of $\Delta O_{2[phy]}$ and $F_{[O_2]_{bio\text{-}as}}$.

While the models we present show promise, more work is needed to estimate $F_{[O_2]_{bio\text{-}as}}$ and NCP from total O_2. Future improvements include (a) reduction in the uncertainty in $\Delta O_{2[phy]}$ measurements by improving optode calibrations, correcting potential biases in the O_2 signal induced by seawater temperature change, bubble effect, and oxygen loss due to the biofilm activity in the ship underway lines (Juranek et al., 2010), and (b) collection of more data to further test the generalizability of our models. The methods proposed here and future modifications may also lead to new insights into drivers of variability in atmospheric potential oxygen. In regions where vertical mixing is negligible or accurately estimated, $F_{[O_2]_{bio\text{-}as}}$ can provide independent estimates of NCP.

Data Availability Statement

All data required to conduct this study are publicly available through the links provided in the Section 2.1.

Acknowledgments

N. Cassar was supported by the "Laboratoire d'Excellence" LabexMER (ANR-10-LABX-19) and co-funded by a grant from the French government under the program "Investissements d'Avenir." Y. Huang was supported by grants from the China NSF (Nos. 42130401 and 42141002). Y. Huang was also partly supported by Chinese State Scholarship Fund to study at Duke University as a joint PhD student (No. 201806310052). R. Eveleth was supported by the NSF GRFP under grant (No. 1106401). D. Nicholson was supported by the NSF OCE-1129973 and OCE-1923915. The data source is presented in Section 2.1. The authors thank the reviewers for their helpful comments. The authors are also grateful to collaborators for contributing their data to this project.

References

Betzer, P. R., Showers, W. J., Laws, E. A., Winn, C. D., DiTullio, G. R., & Kroopnick, P. M. (1984). Primary productivity and particle fluxes on a transect of the equator at 153°W in the Pacific Ocean. *Deep Sea Research Part I: Oceanographic Research Papers*, *31*(1), 1–11. https://doi.org/10.1016/0198-0149(84)90068-2

Boyd, P. W., Claustre, H., Levy, M., Siegel, D. A., & Weber, T. (2019). Multi-faceted particle pumps drive carbon sequestration in the ocean. *Nature*, *568*(7752), 327–335. https://doi.org/10.1038/s41586-019-1098-2

Boyer, T., Baranova, O., Coleman, C., Garcia, H., Grodsky, A., Locarnini, R. A., et al. (2018). World Ocean Database 2018. In A. V. Mishonov (Technical Ed.), *NOAA Atlas NESDIS 87*.

Buesseler, K. O. (1998). The decoupling of production and particulate export in the surface ocean. *Global Biogeochemical Cycles*, *12*(2), 297–310. https://doi.org/10.1029/97GB03366

Bushinsky, S. M., & Emerson, S. (2015). Marine biological production from *in situ* oxygen measurements on a profiling float in the subarctic Pacific Ocean. *Global Biogeochemical Cycles*, *29*(12), 2050–2060. https://doi.org/10.1002/2015gb005251

Cassar, N., Barnett, B. A., Bender, M. L., Kaiser, J., Hamme, R. C., & Tilbrook, B. (2009). Continuous high-frequency dissolved O_2/Ar measurements by equilibrator inlet mass spectrometry. *Analytical Chemistry*, *81*(5), 1855–1864. https://doi.org/10.1021/ac802300u

Cassar, N., Nevison, C. D., & Manizza, M. (2014). Correcting oceanic O_2/Ar-net community production estimates for vertical mixing using N_2O observations. *Geophysical Research Letters*, *41*(24), 8961–8970. https://doi.org/10.1002/2014gl062040

Cassar, N., Nicholson, D., Khatiwala, S., & Cliff, E. (2021). Decomposing the oxygen signal in the ocean interior: Beyond decomposing organic matter. *Geophysical Research Letters*, *48*(18), e2021GL092621. https://doi.org/10.1029/2021gl092621

Chai, F., Johnson, K. S., Claustre, H., Xing, X., Wang, Y., Boss, E., et al. (2020). Monitoring ocean biogeochemistry with autonomous platforms. *Nature Reviews Earth & Environment*, *1*(6), 315–326. https://doi.org/10.1038/s43017-020-0053-y

Claustre, H., Johnson, K. S., & Takeshita, Y. (2020). Observing the global ocean with biogeochemical-Argo. *Annual Review of Marine Science*, *12*(1), 23–48. https://doi.org/10.1146/annurev-marine-010419-010956

Craig, H., & Hayward, T. (1987). Oxygen supersaturation in the ocean: Biological versus physical contributions. *Science*, *235*(4785), 199–202. https://doi.org/10.1126/science.235.4785.199

Ducklow, H. W., & Doney, S. C. (2013). What is the metabolic state of the oligotrophic ocean? A debate. *Annual Review of Marine Science*, *5*(1), 525–533. https://doi.org/10.1146/annurev-marine-121211-172331

Dugdale, R. C., & Goering, J. J. (1967). Uptake of new and regenerated forms of nitrogen in primary productivity. *Limnology & Oceanography*, *12*(2), 196. https://doi.org/10.4319/lo.1967.12.2.0196

Elskens, M., Brion, N., Buesseler, K., Van Mooy, B. A. S., Boyd, P., Dehairs, F., et al. (2008). Primary, new and export production in the NW Pacific subarctic gyre during the vertigo K2 experiments. *Deep Sea Research Part II: Topical Studies in Oceanography*, *55*(14), 1594–1604. https://doi.org/10.1016/j.dsr2.2008.04.013

Emerson, S., Yang, B., White, M., & Cronin, M. (2019). Air-sea gas transfer: Determining bubble fluxes with *in situ* N_2 observations. *Journal of Geophysical Research: Oceans*, *124*(4), 2716–2727. https://doi.org/10.1029/2018jc014786

Eppley, R. W., & Peterson, B. J. (1979). Particulate organic matter flux and planktonic new production in the deep ocean. *Nature*, *282*(5740), 677–680. https://doi.org/10.1038/282677a0

Eveleth, R., Cassar, N., Doney, S. C., Munro, D. R., & Sweeney, C. (2017). Biological and physical controls on O_2/Ar, Ar and pCO_2 variability at the Western Antarctic Peninsula and in the Drake Passage. *Deep Sea Research Part II: Topical Studies in Oceanography*, *139*, 77–88. https://doi.org/10.1016/j.dsr2.2016.05.002

Eveleth, R., Timmermans, M. L., & Cassar, N. (2014). Physical and biological controls on oxygen saturation variability in the upper Arctic Ocean. *Journal of Geophysical Research: Oceans*, *119*(11), 7420–7432. https://doi.org/10.1002/2014jc009816

Field, C. B., Behrenfeld, M. J., Randerson, J. T., & Falkowski, P. (1998). Primary production of the biosphere: Integrating terrestrial and oceanic components. *Science*, *281*(5374), 237–240. https://doi.org/10.1126/science.281.5374.237

Friedlingstein, P., O'Sullivan, M., Jones, M. W., Andrew, R. M., Hauck, J., Olsen, A., et al. (2020). Global carbon budget 2020. *Earth System Science Data*, *12*(4), 3269–3340. https://doi.org/10.5194/essd-12-3269-2020

Garcia, H. E., & Gordon, L. I. (1992). Oxygen solubility in seawater-better fitting equations. *Limnology & Oceanography*, *37*(6), 1307–1312. https://doi.org/10.4319/lo.1992.37.6.1307

Giesbrecht, K. E., Hamme, R. C., & Emerson, S. R. (2012). Biological productivity along Line P in the subarctic northeast Pacific: *In situ* versus incubation-based methods. *Global Biogeochemical Cycles*, *26*(3), 2012GB004349. https://doi.org/10.1029/2012gb004349

Gruber, N., Clement, D., Carter, B. R., Feely, R. A., van Heuven, S., Hoppema, M., et al. (2019). The oceanic sink for anthropogenic CO_2 from 1994 to 2007. *Science*, *363*(6432), 1193–1199. https://doi.org/10.1126/science.aau5153

Hamme, R. C., Cassar, N., Lance, V. P., Vaillancourt, R. D., Bender, M. L., Strutton, P. G., et al. (2012). Dissolved O_2/Ar and other methods reveal rapid changes in productivity during a Lagrangian experiment in the Southern Ocean. *Journal of Geophysical Research*, *117*(C4), C00F12. https://doi.org/10.1029/2011JC007046

Hamme, R. C., & Emerson, S. R. (2004). The solubility of neon, nitrogen and argon in distilled water and seawater. *Deep Sea Research Part I: Oceanographic Research Papers*, *51*(11), 1517–1528. https://doi.org/10.1016/j.dsr.2004.06.009

Hamme, R. C., Nicholson, D. P., Jenkins, W. J., & Emerson, S. R. (2019). Using noble gases to assess the ocean's carbon pumps. *Annual Review of Marine Science*, *11*(1), 75–103. https://doi.org/10.1146/annurev-marine-121916-063604

Huang, Y., Fassbender, A. J., Long, J. S., Johannessen, S., & Bernardi Bif, M. (2022). Partitioning the export of distinct biogenic carbon pools in the Northeast Pacific Ocean using a biogeochemical profiling float. *Global Biogeochemical Cycles*, *36*(2), e2021GB007178. https://doi.org/10.1029/2021gb007178

Huang, Y., Yang, B., Chen, B., Qiu, G., Wang, H., & Huang, B. (2018). Net community production in the South China Sea Basin estimated from *in situ* O_2 measurements on an Argo profiling float. *Deep Sea Research Part I: Oceanographic Research Papers*, *131*, 54–61. https://doi.org/10.1016/j.dsr.2017.11.002

Izett, R. W., & Tortell, P. D. (2021). $\Delta O_2/N_2'$ as a tracer of mixed layer net community production: Theoretical considerations and proof-of-concept. *Limnology and Oceanography: Methods*, *19*(8), 497–509. https://doi.org/10.1002/lom3.10440

Izett, R. W., Hamme, R. C., McNeil, C., Manning, C. C. M., Bourbonnais, A., & Tortell, P. D. (2021). $\Delta O_2/N_2'$ as a new tracer of marine net community production: Application and evaluation in the Subarctic Northeast Pacific and Canadian Arctic Ocean. *Frontiers in Marine Science*, *8*, 718625. https://doi.org/10.3389/fmars.2021.718625

Izett, R. W., Manning, C. C., Hamme, R. C., & Tortell, P. D. (2018). Refined estimates of net community production in the Subarctic Northeast Pacific derived from ΔO_2/Ar measurements with N_2O-based corrections for vertical mixing. *Global Biogeochemical Cycles*, *32*(3), 326–350. https://doi.org/10.1002/2017gb005792

Izett, R. W., & Tortell, P. (2020). The Pressure of In Situ Gases Instrument (PIGI) for autonomous shipboard measurement of dissolved O_2 and N_2 in surface ocean waters. *Oceanography*, *33*(2), 156–162. https://doi.org/10.5670/oceanog.2020.214

Jonsson, B. F., Doney, S. C., Dunne, J., & Bender, M. (2013). Evaluation of the Southern Ocean O_2/Ar-based NCP estimates in a model framework. *Journal of Geophysical Research: Biogeosciences*, *118*(2), 385–399. https://doi.org/10.1002/jgrg.20032

Juranek, L. W., & Quay, P. D. (2005). *In vitro* and *in situ* gross primary and net community production in the North Pacific Subtropical Gyre using labeled and natural abundance isotopes of dissolved O_2. *Global Biogeochemical Cycles*, *19*(3), GB3009. https://doi.org/10.1029/2004gb002384

Juranek, L. W., Hamme, R. C., Kaiser, J., Wanninkhof, R., & Quay, P. D. (2010). Evidence of O_2 consumption in underway seawater lines: Implications for air-sea O_2 and CO_2 fluxes. *Geophysical Research Letters*, *37*(1), L01601. https://doi.org/10.1029/2009gl040423

Juranek, L. W., White, A. E., Dugenne, M., Henderikx Freitas, F., Dutkiewicz, S., Ribalet, F., et al. (2020). The importance of the phytoplankton "middle class" to ocean net community production. *Global Biogeochemical Cycles*, *34*(12), e2020GB006702. https://doi.org/10.1029/2020gb006702

Kalnay, E., Kanamitsu, M., Kistler, R., Collins, W., Deaven, D., Gandin, L., et al. (1996). The NCEP/NCAR 40-year reanalysis project. *Bulletin of the American Meteorological Society*, *77*(3), 437–471. https://doi.org/10.1175/1520-0477(1996)077<0437:tnyrp>2.0.co;2

Keeling, R. F. (1993). On the role of large bubbles in air-sea gas exchange and supersaturation in the ocean. *Journal of Marine Research*, *51*(2), 237–271. https://doi.org/10.1357/0022240933223800

Khatiwala, S. (2007). A computational framework for simulation of biogeochemical tracers in the ocean. *Global Biogeochemical Cycles*, *21*(3), GB3001. https://doi.org/10.1029/2007gb002923

Koza, J. R. (1994). Genetic programming as a means for programming computers by natural selection. *Statistics and Computing*, *4*, 87–112. https://doi.org/10.1007/BF00175355

Laws, E. A. (1991). Photosynthetic quotients, new production and net community production in the open ocean. *Deep-Sea Research, Part A: Oceanographic Research Papers*, *38*(1), 143–167. https://doi.org/10.1016/0198-0149(91)90059-O

Laws, E. A., D'Sa, E., & Naik, P. (2011). Simple equations to estimate ratios of new or export production to total production from satellite-derived estimates of sea surface temperature and primary production. *Limnology and Oceanography: Methods*, *9*(12), 593–601. https://doi.org/10.4319/lom.2011.9.593

Li, Z., & Cassar, N. (2016). Satellite estimates of net community production based on O_2/Ar observations and comparison to other estimates. *Global Biogeochemical Cycles*, *30*(5), 735–752. https://doi.org/10.1002/2015GB005314

Li, Z., & Cassar, N. (2017). A mechanistic model of an upper bound on oceanic carbon export as a function of mixed layer depth and temperature. *Biogeosciences*, *14*(22), 5015–5027. https://doi.org/10.5194/bg-14-5015-2017

Liang, J.-H., Deutsch, C., McWilliams, J. C., Baschek, B., Sullivan, P. P., & Chiba, D. (2013). Parameterizing bubble-mediated air-sea gas exchange and its effect on ocean ventilation. *Global Biogeochemical Cycles*, *27*(3), 894–905. https://doi.org/10.1002/gbc.20080

Liang, J.-H., Emerson, S. R., D'Asaro, E. A., McNeil, C. L., Harcourt, R. R., Sullivan, P. P., et al. (2017). On the role of sea-state in bubble-mediated air-sea gas flux during a winter storm. *Journal of Geophysical Research: Oceans*, *122*(4), 2671–2685. https://doi.org/10.1002/2016jc012408

Luz, B., & Barkan, E. (2009). Net and gross oxygen production from O_2/Ar, $^{17}O/^{16}O$ and $^{18}O/^{16}O$ ratios. *Aquatic Microbial Ecology*, *56*, 133–145. https://doi.org/10.3354/ame01296

Millero, F. J., Perron, G., & Desnoyers, J. (1973). Heat capacity of seawater solutions from 5° to 35°C and 0.5 to 22‰ chlorinity. *Journal of Geophysical Research*, *78*(21), 4499–4507. https://doi.org/10.1029/JC078i021p04499

Murray, J. W., Young, J., Newton, J., Dunne, J., Chapin, T., Paul, B., & McCarthy, J. J. (1996). Export flux of particulate organic carbon from the central equatorial Pacific determined using a combined drifting trap-^{234}Th approach. *Deep Sea Research Part II: Topical Studies in Oceanography*, *43*(4), 1095–1132. https://doi.org/10.1016/0967-0645(96)00036-7

Nevison, C. D., Keeling, R. F., Kahru, M., Manizza, M., Mitchell, B. G., & Cassar, N. (2012). Estimating net community production in the Southern Ocean based on atmospheric potential oxygen and satellite ocean color data. *Global Biogeochemical Cycles*, *26*(1), GB1020. https://doi.org/10.1029/2011gb004040

Nevison, C., Munro, D., Lovenduski, N., Cassar, N., Keeling, R., Krummel, P., & Tjiputra, J. (2018). Net community production in the Southern Ocean: Insights from comparing atmospheric potential oxygen to satellite ocean color algorithms and ocean models. *Geophysical Research Letters*, *45*(19), 10–549. https://doi.org/10.1029/2018gl079575

Nicholson, D. P., Emerson, S. R., Khatiwala, S., & Hamme, R. C. (2011). An inverse approach to estimate bubble-mediated air-sea gas flux from inert gas measurements. In *Paper presented at Proceedings on the 6th International Symposium on Gas Transfer at Water Surfaces*. Kyoto University Press.

Nicholson, D. P., Khatiwala, S., & Heimbach, P. (2016). Noble gas tracers of ventilation during deep-water formation in the Weddell Sea. *IOP Conference Series: Earth and Environmental Science*, *35*, 012019. https://doi.org/10.1088/1755-1315/35/1/012019

Plant, J. N., Johnson, K. S., Sakamoto, C. M., Jannasch, H. W., Coletti, L. J., Riser, S. C., & Swift, D. D. (2016). Net community production at Ocean Station Papa observed with nitrate and oxygen sensors on profiling floats. *Global Biogeochemical Cycles*, *30*(6), 859–879. https://doi.org/10.1002/2015gb005349

Quay, P. D., Peacock, C., Björkman, K., & Karl, D. M. (2010). Measuring primary production rates in the ocean: Enigmatic results between incubation and non-incubation methods at Station ALOHA. *Global Biogeochemical Cycles*, *24*(3), GB3014. https://doi.org/10.1029/2009GB003665

R Core Team. (2014). A language and environment for statistical computing. R Foundation for Statistical Computing.

Sarma, V. V. S. S. (2004). Net plankton community production in the Arabian Sea based on O_2 mass balance model. *Global Biogeochemical Cycles*, *18*(4), GB4001. https://doi.org/10.1029/2003gb002198

Schmidtko, S., Stramma, L., & Visbeck, M. (2017). Decline in global oceanic oxygen content during the past five decades. *Nature*, *542*(7641), 335–339. https://doi.org/10.1038/nature21399

Serret, P., Robinson, C., Fernández, E., Teira, E., & Tilstone, G. (2001). Latitudinal variation of the balance between plankton photosynthesis and respiration in the eastern Atlantic Ocean. *Limnology & Oceanography*, *46*(7), 1642–1652. https://doi.org/10.4319/lo.2001.46.7.1642

Sigman, D. M., & Boyle, E. A. (2000). Glacial/interglacial variations in atmospheric carbon dioxide. *Nature*, *407*(6806), 859–869. https://doi.org/10.1038/35038000

Spitzer, W. S., & Jenkins, W. J. (1989). Rates of vertical mixing, gas exchange and new production: Estimates from seasonal gas cycles in the upper ocean near Bermuda. *Journal of Marine Research*, *47*(1), 169–196. https://doi.org/10.1357/002224089785076370

Stanley, R. H. R., Jenkins, W. J., Lott, D. E., Iii, & Doney, S. C. (2009). Noble gas constraints on air-sea gas exchange and bubble fluxes. *Journal of Geophysical Research*, *114*(C11), C11020. https://doi.org/10.1029/2009JC005396

Tandon, A., & Zahariev, K. (2001). Quantifying the role of mixed layer entrainment for water mass transformation in the North Atlantic. *Journal of Physical Oceanography*, *31*(4), 1120–1131. https://doi.org/10.1175/1520-0485(2001)031<1120:Qtroml>2.0.Co;2

Tang, W., Wang, S., Fonseca-Batista, D., Dehairs, F., Gifford, S., Gonzalez, A. G., et al. (2019). Revisiting the distribution of oceanic N_2 fixation and estimating diazotrophic contribution to marine production. *Nature Communications*, *10*(1), 831. https://doi.org/10.1038/s41467-019-08640-0

Teeter, L., Hamme, R. C., Ianson, D., & Bianucci, L. (2018). Accurate estimation of net community production from O_2/Ar measurements. *Global Biogeochemical Cycles*, *32*, 1163–1181. https://doi.org/10.1029/2017gb005874

Tilstone, G. H., Xie, Y.-y., Robinson, C., Serret, P., Raitsos, D. E., Powell, T., et al. (2015). Satellite estimates of net community production indicate predominance of net autotrophy in the Atlantic Ocean. *Remote Sensing of Environment*, *164*, 254–269. https://doi.org/10.1016/j.rse.2015.03.017

Timmerman, A. H. V. & Hamme, R. C. (2021). Consistent relationships among productivity rate methods in the NE subarctic Pacific. *Global Biogeochemical Cycles*. https://doi.org/10.1029/2020gb006721

Volk, T., & Hoffert, M. I. (1985). Ocean carbon pumps: Analysis of relative strengths and efficiencies in ocean-driven atmospheric CO_2 changes. In *The carbon cycle and atmospheric CO_2: Natural variations Archean to present*. https://doi.org/10.1029/GM032p0099

Wallcraft, A. J., Kara, A. B., Hurlburt, H. E., Chassignet, E. P., & Halliwell, G. H. (2008). Value of bulk heat flux parameterizations for ocean SST prediction. *Journal of Marine Systems*, *74*(1), 241–258. https://doi.org/10.1016/j.jmarsys.2008.01.009

Wang, S., Kranz, S. A., Kelly, T. B., Song, H., Stukel, M. R., & Cassar, N. (2020). Lagrangian studies of net community production: The effect of diel and multi-day non-steady state factors and vertical fluxes on O_2/Ar in a dynamic upwelling region. *Journal of Geophysical Research: Biogeosciences*, *125*(6), e2019JG005569. https://doi.org/10.1029/2019jg005569

Wang, S., Lin, Y., Gifford, S., Eveleth, R., & Cassar, N. (2018). Linking patterns of net community production and marine microbial community structure in the western North Atlantic. *The ISME Journal*, *12*(11), 2582–2595. https://doi.org/10.1038/s41396-018-0163-4

Wanninkhof, R. (2014). Relationship between wind speed and gas exchange over the ocean revisited. *Limnology and Oceanography: Methods*, *12*(6), 351–362. https://doi.org/10.4319/lom.2014.12.351

Weiss, R. F., & Price, B. A. (1980). Nitrous oxide solubility in water and seawater. *Marine Chemistry*, *8*(4), 347–359. https://doi.org/10.1016/0304-4203(80)90024-9

Westberry, T., Behrenfeld, M. J., Siegel, D. A., & Boss, E. (2008). Carbon-based primary productivity modeling with vertically resolved photoacclimation. *Global Biogeochemical Cycles*, *22*(2), 85. https://doi.org/10.1029/2007gb003078

Williams, P. J. L., & Purdie, D. A. (1991). *In vitro* and *in situ* derived rates of gross production, net community production and respiration of oxygen in the oligotrophic subtropical gyre of the North Pacific Ocean. *Deep-Sea Research, Part A: Oceanographic Research Papers*, *38*(7), 891–910. https://doi.org/10.1016/0198-0149(91)90024-a

Wyrtki, K. (1981). An estimate of equatorial upwelling in the Pacific. *Journal of Physical Oceanography*, *11*(9), 1205–1214. https://doi.org/10.1175/1520-0485(1981)011<1205:Aeoeui>2.0.Co;2

References From the Supporting Information

Gade, K. (2010). A non-singular horizontal position representation. *Journal of Navigation*, *63*(3), 395–417. https://doi.org/10.1017/S0373463309990415